Damage characterization in laminated composites by measuring the displacement field

Farge L.[1] Varna J.[2] and , Ayadi Z.[1]

[1] Laboratoire de Science et Génie des Surfaces - Institut Jean Lamour, EEIGM 6 Rue Bastien Lepage, F-54010 Nancy Cedex, France.
[2] Division of Polymer Engineering, Luleå University of Technology, SE-971 87 Luleå, Sweden.

ABSTRACT

Using Electronic Speckle Pattern Interferometry (ESPI), the full-field displacement measurement was obtained on the edge of a cracked laminate subjected to a tensile loading. The displacement jumps corresponding to cracks are clearly visible and can be used to determine the Crack Opening Displacement (*COD*) values along the cracks. The main objective of this study is to determine if the application of high load may have modified the existing cracks and consequently changed the *COD* dependence on the applied stress. The profile of the opening was also studied.

1. INTRODUCTION

Microcracks develop in off-axis plies of laminates subjected to thermo-mechanical loading. Usually they are matrix and interface related intralaminar cracks with a crack plane transverse to the laminate midplane (see Fig. 1). The level of degradation of thermo-mechanical constants of composite laminates due to microcracks in layers is related to the laminate lay-up, the number of cracks and the geometry of these cracks. The geometry (straight idealized cracks, cracks with local delaminations at the crack tip etc. …) has effect on the stress state between two cracks which governs development of new cracks and the load bearing efficiency of the damaged layer. If at fixed applied strain the crack face opening displacements (*COD*) and the sliding displacements (*CSD*), defined as the relative displacements of the corresponding points at both crack surfaces, are large the average stress between these cracks is low. For example, delaminations at the intralaminar crack tip lead to larger *COD* as compared to ideal "sharp" cracks at the same applied load. Detection and quantification of local delaminations is not a straightforward task and full field train measurements may be a useful tool for their characterization.

The link between the damaged laminate thermo-elastic constants and the microdamage parameters (crack density, crack face opening displacements (*COD*) and crack face sliding displacements (*CSD*)) was established by Lundmark et al [1,2] and Gudmundson. et al.[3]. It was shown that only the average values of *COD* and *CSD* enter the stiffness expressions directly. In a linear solution the average *COD* and *CSD* values are proportional to the applied load and, therefore, they have to be normalized to be used in stiffness modeling. Thus the two components of the relative in-plane displacement of the crack faces: the average normalized *COD* and the average normalized *CSD* are the micromechanical parameters governing the macroscopic stiffness reduction.

In principle, the experimental determination of the average *COD* and *CSD* needs the measurement of the displacement for every points on the crack surfaces, which justifies the use of full-field measurement techniques.

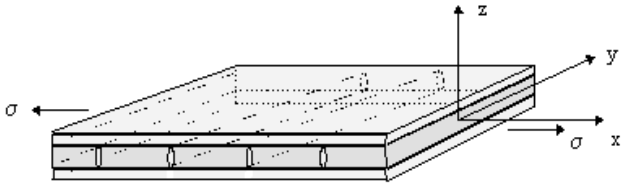

Figure 1: Schematic showing of a laminate with transverse cracks in the middle layer. The laminate is subjected to a tensile loading along the x-axis.

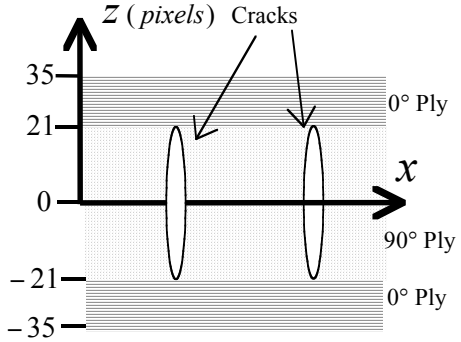

Figure 2: Schematic view of the laminate. z-axis corresponds to the laminate thickness direction. x-axis is the tensile direction. $z = 0$ corresponds to the midplane. ($1\,pixel = 18.26\mu m$, laminate thickness: $1.28\,mm$, laminate width: $20\,mm$).

Using ESPI (Electronic Speckle Pattern Interferometry), an optical measurement tool that provides non-contact displacement measurement at every point on a surface [4,5], the displacement field was obtained on the edge of the laminate with multiple cracks in its central layer. The cracks logically appear as singularities in the displacement field [6] and the corresponding displacement jumps are directly related to *COD* and *CSD* [7]. In [6] the *COD* dependence on the applied stress was analyzed. In particular, we studied if the application of an additional loading (higher than the initial loading used to create the cracks) modifies the existing cracks, changing the normalized *COD* value. With the aim of evaluating the average *COD*, we also studied the profile of the COD.

2. MATERIAL AND LOADING HISTORY

The $[0_2,90_3]$s laminate (see the geometrical details in Figure 2) was made of toughened carbon fiber/epoxy (AS4/8552) unidirectional tape prepreg using vacuum bag technique.

Fig. 3 shows the loading history corresponding to the application of a tensile strain along the x-axis. After Loading_1 (first damage state) some cracks were created in the 90^0 ply. The first *COD* measurements were carried out at this first damage state. The specimen was subsequently subjected to a second loading (Loading_2) of higher level, leading to the second damage state. Another measurement run was carried out at this second damage state (Fig. 3).

Let us note that the crack being parallel to the fiber direction (i.e in a $90°$ direction with respect to the tensile direction), there is no relative sliding of the crack faces. The only displacement of the crack faces is therefore COD.

The effcetive strain in the specimen was obtained using extensometer.

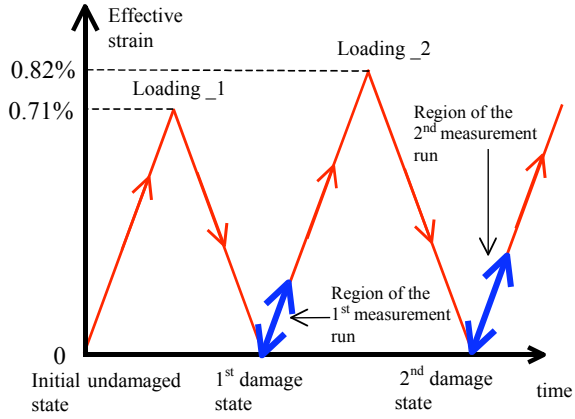

Figure 3: Loading history.

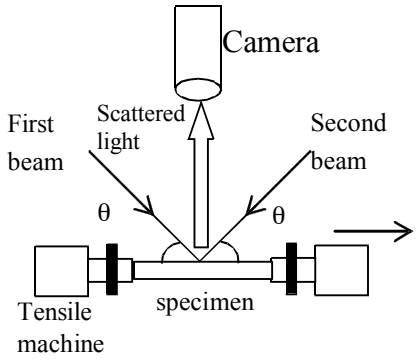

Figure 4: Experimental arrangement.

3. MEASUREMENT PRINCIPLE, ESPI

If a surface is illuminated by a coherent beam, the surface roughness causes multiple phase differences that create random interference. Hence, the sensor of a camera collects a randomly distributed distribution of light intensity called speckle. If a point of the surface is subjected to a displacement, the local speckle pattern undergoes the same displacement.

The experimental set up used in that work corresponds to the well-known Leendertz arrangement [8] (Figure 4). The surface is illuminated by two beams that form the same angle θ with respect to the studied surface. The corresponding speckle patterns also interfere. The resulting light intensity is given by [4,9]

$$I_1 = I_0(x,y) + I_M(x,y)\cos(\phi(x,y)) \qquad (1)$$

I_0, I_M and ϕ are respectively the background intensity, the modulation intensity and the phase, which is a modulo 2π random number.

In order to implement the phase-shifting technique [10,11], a piezoelectric device makes it possible to introduce a $\pi/2$ phase shift in one of the two beams. The intensity images I_0, I_1, I_2, I_3, and I_4 corresponding to phase shifts of respectively 0, $\pi/2$, π, $3\pi/2$, 2π are recorded so that the phase maps can be calculated using the following equation:

$$\phi = \tan^{-1}\left(\frac{2(I_3 - I_1)}{I_4 + I_0 - 2I_2}\right) \qquad (2)$$

Let $u(x,z)$ be the relative displacement along the x-axis corresponding to a passage from an initial loading state to a final loading state. It is directly linked to the phase difference between these two states:

$$\phi_{\mathbf{final}} - \phi_{\mathbf{initial}} = (4\partial \cos(\theta) u(x,z))/\ddot{e} \qquad (3)$$

$\lambda = 633nm$ is the laser wavelength.

The cracks correspond to discontinuities of this phase difference at the crack locations [12].

Thus the recordings of the phase maps for the initial and the final states allows to obtain the relative displacement $u(x,z)$ for every point of the specimen surface (e.g. Fig. 5). This displacement corresponds to a $\Delta\sigma$ increase of the effective stress applied to the specimen.

If the displacement jumps corresponding to cracks are too important, they can make it impossible to detect the mathematical discontinuities of the function $\tan^{-1}$. A satisfying phase unwrapping is then impossible [4]. This problem did not occur if the relative displacements were kept smaller than $2\mu m$ in the region of study.

In order to reduce the measurement noise, the phase maps were averaged using a [5 pixels×5 pixels] filtering kernel. The pixel size being $18.26\mu m$, it approximately corresponds to a $90\mu m$ value for the spatial resolution.

4. CRACK OPENING DISPLACEMENT MEASUREMENTS AT THE FIRST DAMAGED STATE

The first measurement was carried out just after Loading 1, it corresponds to the first damaged state (see Fig. 3). In order not to introduce new damage, the measurements were made for values of the average strain that do not exceed 0.080%.

Fig. 5 shows an example of a displacement map and of a displacement profile for $z = 0$ (i.e. on the midplane). Four displacement jumps can be seen on this profile. These displacement jumps naturally indicate the presence of four cracks in the region of study. The displacement slope (strain) is smaller in the area at the vicinity of the crack surfaces (points A_i). It is consistent with the boundary condition with stress free microcrack surfaces.

Fig. 6 corresponds to profiles drawn along the midplane and in the 0° ply ($z = +30\ pixels$). No displacement jumps can be seen in the $0°$ ply, which is in agreement with what is expected for the crack localization in the plies (Fig. 2).

Using displacement profiles similar to the one shown on Fig. 5, the COD values were measured on the midplane for each crack.

Measurements with the same initial and final load levels were repeated 6 times. The value of the normalized COD with respect to the effective stress increment is given by $COD^1_{nor} = \dfrac{COD}{\Delta\sigma}$, $\Delta\sigma$ being the effective stress increment.

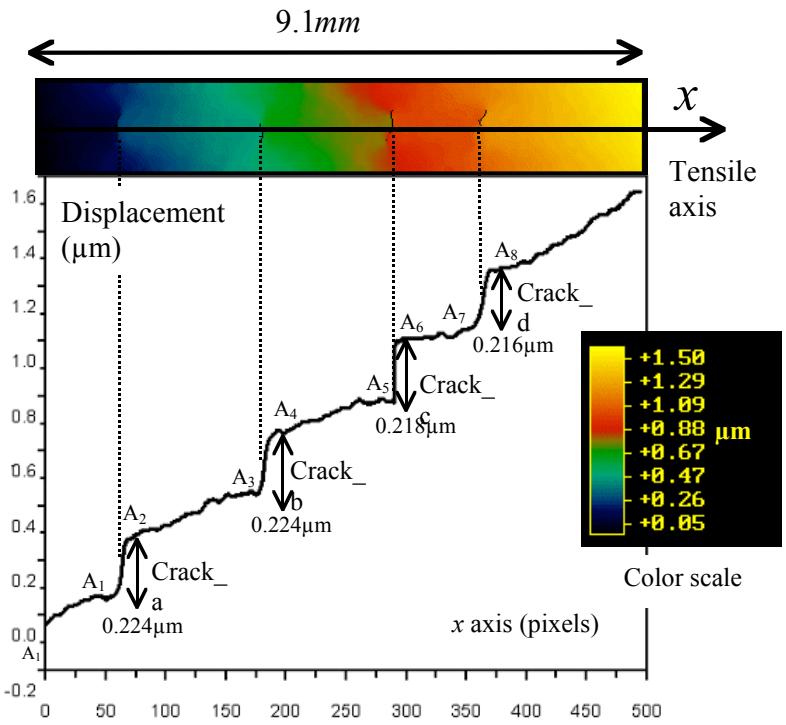

Figure 5: Displacement map and displacement profile on the midplane ($z = 0$). ($1\,pixel = 18.26\mu m$, $\Delta\sigma \in [23.47MPa, 35.27MPa]$). For each crack, the COD values are indicated.

Table 1: Mean and standard deviation of the normalized crack opening displacement on the midplane at the first damage state. All measurements were made for the same effective stress increment: $\Delta\sigma \in [19.53MPa, 31.25MPa]$.

Measurements at the 1st damaged state	Crack_a	Crack_b	Crack_c	Crack_d
$\overline{COD^1_{nor}}$: mean of 6 measurements for COD^1_{nor} ($\mu m MPa^{-1}$).	0.0187	0.0176	0.0186	0.0182
Standard deviation of the measurements for COD_n ($\mu m MPa^{-1}$).	0.00053	0.00088	0.00057	0.00061

Subscript 1 indicates that the measurement corresponds to the first damage state. The mean of the 6 COD^1_{nor} values is denoted $\overline{COD^1_{nor}}$. For each crack, the values of $\overline{COD^1_{nor}}$ are listed on Table 1. Let us note that the standard deviations shown on Table 1 provide an estimate of the measurement accuracy.

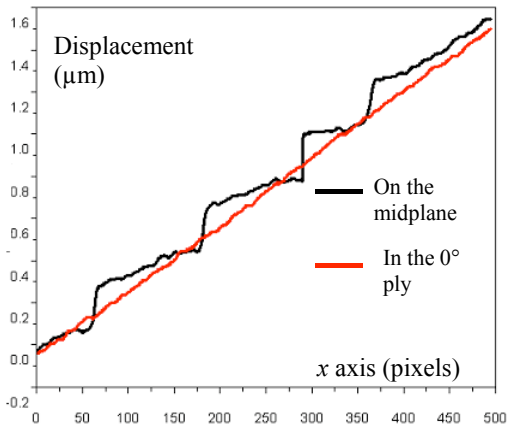

Figure 6: Displacement profiles on the midplane and in the 0° ply.
($1\,pixel = 18.26\mu m$,
$\Delta\sigma \in [23.47MPa, 35.27MPa]$)

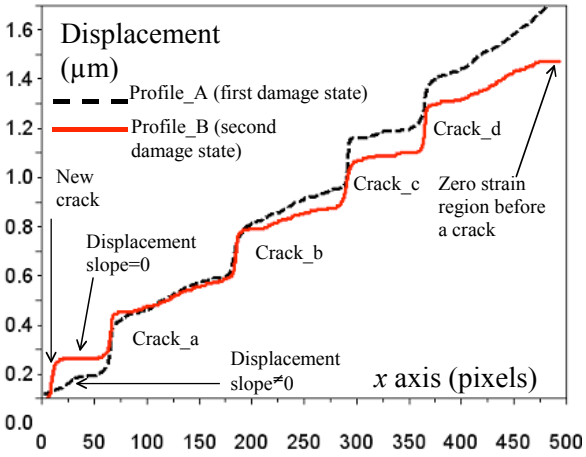

Figure 7: Displacement profiles along the x—axis. The two profiles are taken on the midplane. They correspond to measurements at the first and at the second damage state.
($1\,pixel = 18.26\mu m$,
$\Delta\sigma \in [19.53MPa, 31.25MPa]$)

5. CRACK OPENING DISPLACEMENT MEASUREMENTS AT THE SECOND DAMAGE STATE

The objective of this part is to analyze how an additional loading could introduce new damage. A loading corresponding to a higher level of the average strain may indeed either create new cracks or modify the existing cracks; witch would eventually result in a change of the normalized COD value.

The specimen was therefore subjected to a second loading that has a higher level than the initial one. This additional loading is denoted Loading_2 on Fig. 3. Fig. 7 shows the displacement profiles corresponding to measurements that were made before (Profile_A) and after Loading_2 (Profile_B). At the left part of the figure, a new displacement jump can be seen on Profile_B, which certainly corresponds to a new crack generated by Loading_2. On Profile_2, the displacement curve appears to be flat between the new crack and Crack_a. It results from the stress free boundary condition at the surfaces of these two close cracks. On the other hand, the displacement slope corresponding to the same region has a non zero value for Profile_A. It is naturally due to the absence of a crack at the left of Crack_a before the application of Loading_2. The total displacement corresponding to Profile_A is larger than the one corresponding to Profile_B. It may be explained by another new crack created at the right just outside the region of study. The zero strain region that is on the left face of this new crack can indeed be discerned at the right side of Profile_B. It can be assumed that the displacement jump corresponding to this crack is likely to compensate the gap between the two curves. For each crack, Table 2 shows the values of $\overline{COD_{nor}^2}$, which is the mean of the COD_{nor} values at the second damage state.

The measurement conditions are the same as in Table 1: the same person that determines the COD values on the profile, same test number and same initial and final loading forces.

Table 2: Mean and standard deviation of the normalized crack opening displacemen on the midplane at the second damage state. All measurements were made for the same load increment: $\Delta\sigma \in [19.53MPa, 31.25MPa]$

Measurements at the 2nd damaged state	Crack_a	Crack_b	Crack_c	Crack_d
$\overline{COD^2_{nor}}$: mean of 6 the measurements for COD_{nor} ($\mu m MPa^{-1}$)	0.0160	0.0182	0.0177	0.0180
Standard deviation of the measurements for COD_{nor} ($\mu m MPa^{-1}$)	0.00031	0.00066	0.00040	0.00051

For each crack, a Student statistical test was carried out in order to determine if the normalized crack opening displacement has changed after the application of loading_2. The Student tests shows that, from a statistical point of view, $\overline{COD^1_{nor}} = \overline{COD^2_{nor}}$ for Crack_b and Crack_d. Using a low significance level (about 1%), this equation remains true for Crack_c. On the other hand, for Crack_a, the Student test renders without any doubt: $\overline{COD^1_{nor}} \neq \overline{COD^2_{nor}}$. In that last case, the reduction of the normalized crack opening displacement is certainly due to the creation of a new crack at the close vicinity of Crack_a. Actually, if the crack density is high, the stress perturbations of two neighboring cracks start to interact and the average stress between cracks at the given applied load is lower. It means that the COD of interacting cracks are smaller than for non-interactive cracks.

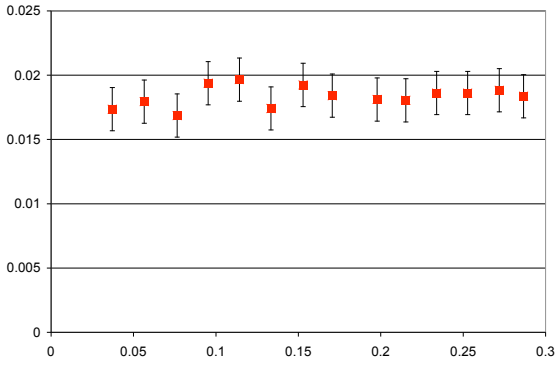

Figure 8: Normalized crack opening displacement (COD^c_{nor}) against total average strain for Crack_c.

In a linear solution, COD is proportional to the applied load, therefore, this quantity has to be normalized to be used in stiffness modeling. In order to test the proportionality with the applied load, we studied the evolution of the normalized COD as a function of the effective strain. The loading was increased by successive $\Delta\sigma$ increments of the effective stress. Fig. 8 shows the obtained results for the normalized crack opening displacement corresponding to Crack_c (COD^{c}_{nor}). The measurement was carried out up to a 0.3% value of the effective strain. This value is smaller than the maximum effective strain corresponding to Loading_2, which should insure that no new damage develop in the laminate during the measurement. Fig. 8 shows that the normalized COD remains constant, which justifies the use of this quantity in the stiffness reduction models. The vertical bars on the measurement points are of the order of the measurement uncertainty. Identical results were obtained for other cracks.

6. CRACK OPENING PROFILE ALONG THE CRACK

It is often assumed (and proved for ideal straight cracks using FEM) that the crack profile is almost elliptical. The knowledge of the displacement at every points of the specimen edge, in particular at the crack surfaces, makes it possible to test the validity of this assumption. The profiles obtained for different values of the z coordinate allow one's to obtain the value of COD along the crack (Fig. 9). It is easy to show that, if a crack has an elliptical shape, the COD obtained using ESPI, which is in fact a relative displacement, follows the same elliptical law. For Crack_c, the following results were obtained: At the upper part (Fig. 2) of the specimen edge ($z \geq 0$): $COD = 0.218\,\mu m$ at $z = 0\,pixel$, $COD = 0.209\,\mu m$ at $z = 5\,pixels$, $COD = 0.200\,\mu m$ at $z = 10\,pixels$ and $COD = 0.162\,\mu m$ at $z = 15\,pixel$.

At the lower part (Fig. 2) of the specimen edge ($z \leq 0$): $COD = 0.218\,\mu m$ at $z = 0\,pixel$, $COD = 0.211\,\mu m$ at $z = -5\,pixels$, $COD = 0.192\,\mu m$ at $z = -10\,pixels$ and $COD = 0.125\,\mu m$ at $z = -15\,pixels$.

The last profiles ($z = \pm 15\,pixels$) was chosen so that, taking into account the filtering kernel size, no pixel in the 0° ply would be involved in the displacement measurement. Fig. 10 corresponds to COD as a function of the z coordinate. In other words, it is the profile of the opening along the crack. On this figure the values of the crack opening displacements correspond to the average between the COD values measured at the top and at the lower parts of the specimen edge (Fig. 2). For example, for $z = 5\,pixels$, $COD = \dfrac{0.209 + 0.211}{2} = 0.210\,\mu m$.

On Fig. 10, the curve corresponds to the equation of an ellipse:

$$COD(Z) = COD(0)\sqrt{1 - (\frac{z}{a})^2} \qquad (4)$$

$COD(0)$ is the value of COD for $z = 0$ (horizontal axis of the schematic ellipse representing the crack on Fig. 2). a is the half length of the crack. (vertical axis of the schematic ellipse representing the crack on Fig. 8)

With the aim of estimating the parameters $COD(0)$ and a, the experimental data was fitted by eq (4). For Crack_c, the obtained results are: $COD(0) = 0.221\mu m$ and $a = 20.25\ Pixels$.

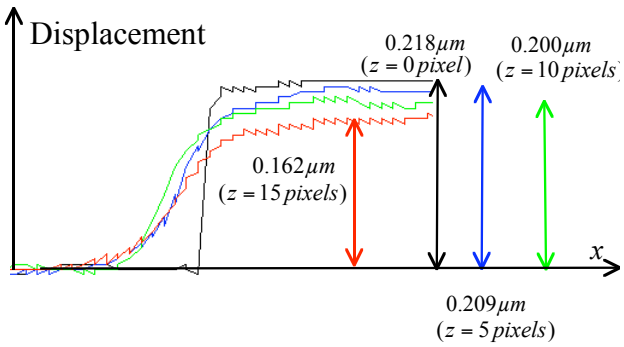

Figure 9: Displacement profiles corresponding to Crack_c for $z = 0\,pixel$, $z = 5\,pixels$, $z = 10\,pixels$ and $z = 15\,pixels$. ($1\,pixel = 18.26\mu m$, $\Delta\sigma \in [23.47MPa, 35.27MPa]$)

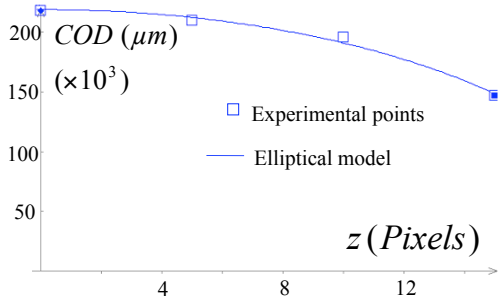

Fig 10: COD profile along the specimen thickness. ($1\,pixel = 18.26\mu m$, $\Delta\sigma \in [23.47MPa, 35.27MPa]$).

An identical analysis was performed for the other cracks: For Crack_a: $COD(0) = 0.223\mu m$, $a = 20.6\ Pixels$, for Crack_b: $COD(0) = 0.224\mu m$, $a = 20.0\ Pixels$, for Crack_d: $COD(0) = 0.215\mu m$, $a = 21.2\ Pixels$. The $COD(0)$ values found by the fitting process are in good agreement with the values of $COD(0)$ measured on the midplane (see Fig. 5), which is naturally good but not very surprising since $COD(0)$ is one of the experimental point used for the data fitting. On the other hand the expected value for the half length of the crack is $a = 21\,pixel$, which is the half-thickness of the cracked ply (Fig. 2). In that latter case, the agreement with the fitted values is very satisfying, taking into that the expected value of a is not used during the fitting process.

The validity of an elliptical model for the COD profile along the crack facilitates the determination of COD^a, average value of the crack opening displacement, which is the parameter used by stiffness reduction models. Assuming an elliptical shape for the crack opening, COD^a can indeed be found starting from a unique COD measurement. For example: $COD^a = \pi/4\,COD(0)$. Due to the averaging with a 5 pixels filtering kernel, the displacement profiles are not taken on a straight line but on a five pixel width strip. Consequently, the COD values are slightly underestimated. Nevertheless, assuming an elliptical shape for the crack opening the error for $z \le 15$ is smaller than 1%.

7. CONCLUSIONS

Displacement measurements at the edge of cross-ply laminate with cracks showed that in the strain range of investigation the normalized COD does not depend on the level of strain previously applied to the laminate and neither on the stress level during full-field

measurements. The first result suggests that no new damage (for example delamination at the crack tips) was initiated at the crack scale. In that case, the change of the crack density may then be considered as the initial cause for the stiffness reduction. The second result proves that linear elasticity is applicable in the high local stress region between cracks.

It was also shown that the opening profiles along the cracks can be considered as elliptical.

This work highlights the usefulness of ESPI for applications that need both high measurement sensitivity and fine spatial resolution.

8. REFERENCES

1. Lundmark P. and Varna, J., "Constitutive relationships for damaged laminate in in-plane loading", *Int J Dam Mech*, 2005; 14 (3):235-259.

2. Lundmark P. and Varna J., "Crack face sliding effect on stiffness of laminates with ply cracks", *Composites Science and Technology*, 2006; 66:1444-1454.

3. Gudmundson P. and Östlund S. "First order analysis of stiffness reduction due to matrix cracking", *J Comp Mater*, 1992; 26:1009-1030.

4. Rastogadi P.K., "Digital pattern interferometry and related techniques", Wiley editor, Chichester, 2001.

5. Jones R., "The design and application of a speckle pattern interferometer for total strain field measurement", *Optics and Laser Technology*, 1976; 8 (5):215-219.

6. Grédiac M., "The use of full-field measurement methods in composite material characterization: interests and limitations", *Composites: part A*, 2004; 35:751-761.

7. Farge L., Ayadi Z. and Varna J., "Optically measured full-field displacement on the edge of a cracked composite laminate", *Composites: Part A*, 2008, in Press, doi: 10.1016/j.compositesa.2007.11.010.

8. Leendertz, J.A., "Interferometric measurement on scattering surfaces using speckle effect", *Journal of Physics E: Scientific Instruments*, 1970, 3:214-218.

9. Moore A.J. and Tyrer J.R., "An electronic speckle pattern interferometer for complete in plane displacement measurement", *Measurement, Science and Technology*, 1990; 1:1024-1030.

10. Moore A.J.and Tyrer J.R, "Two-dimensional strain measurement with ESPI", *Optics and laser Engineering*, 1996; 24:381-402.

11. Nakadate S. and Saito H., "Fringe scanning speckle interferometry", *Applied Optics*, 1985; 24 (14):2172-2180.

12. Avril S., Vautrin A.and Surrel T., "Grid Methods: Application to the characterisation of cracks", *Experimental Mechanics*, 2004, 44 (1):37-43.